Indian Journal of Chemistry
Vol. 64, October 2025, pp. 966-978
DOI: 10.56042/ijc.v64i10.20262

Synthesis, characterization, spectroscopic, DFT, antimicrobial and molecular docking analysis of butane-2,3-dione dioxime and its zinc (II) complex

Reema Chand*[a], Mohseen Ahmed[a] & Bibhesh K Singh[b]

[a] Department of Chemistry, M.B.G.P.G College, Haldwani 263 139, Nainital, Uttarakhand, India

[b] Department of Chemistry, Govt. Degree College, Chamoli 246 487, Uttrakhand, India

E-mail: reemachand292@gmail.com

Received 2 June 2025; accepted (revised) 25 September 2025

This study clarifies the structure of butane-2,3-dione dioxime and its Zn(II) complex through synthesis, characterization, and biological evaluation. The study also aims to clarify its spectroscopic and computational properties. FT-IR analysis confirms that oxime nitrogen binds to Zn(II), and UV-Vis spectroscopy shows that ligand-to-metal charge transfer (LMCT) and electronic transition shifts happen when the two are combined. Powder X-ray diffraction (PXRD) analysis shows that the Zn(II) complex changes from an orthorhombic (Pnmm) to a monoclinic (P21/n) system, with the P21/n system having more crystals. The NMR spectrum shows big downfield shifts in oxime protons and carbons, which supports the idea that the metal and ligand interact. SEM analysis highlights morphological transformations, confirming successful coordination. Mass spectrometry validates molecular composition and fragmentation patterns. According to Density Functional Theory (DFT) calculations, the HOMO-LUMO gaps get smaller when the molecules combine, which means that the electrons move around and react more. Molecular docking studies show that the ligand binds more strongly to anticancer (PDB: 1T46) and antioxidant (PDB: 1HD2) proteins than to its metal complex. Antimicrobial assays show that the ligand exhibits superior antibacterial and antifungal activities.

Keywords: Transition metal complexes, Oxime ligand, DFT calculation, Spectro-thermal characterization, Antimicrobial studies, Molecular docking

Oxime-based ligands have gained considerable attention in coordination chemistry due to their strong metal-chelating ability, diverse coordination modes, and potential biological applications[1]. Among these, butane-2,3-dione dioxime, a vicinal dioxime, is particularly interesting due to its ability to form stable metal complexes, especially with transition metals like Zn(II). Zinc plays a vital role in various biological processes, including enzymatic reactions, DNA synthesis, and immune regulation, making its complexes promising candidates for drug development[2]. Zn(II) complexes are widely explored for their bioactive properties, including antibacterial, antifungal, antioxidant, and anticancer activities, attributed to their ability to interact with biomolecules and influence cellular pathways[3]. Recent studies have highlighted the potential of Zn(II)-oxime complexes in medicinal chemistry, demonstrating enhanced antimicrobial activity, often surpassing conventional antibiotics[4]. Moreover, Density Functional Theory (DFT) and molecular docking studies have provided valuable insights into the electronic structure, stability, and biomolecular interactions of such metal-ligand systems[5]. The structure-activity relationship (SAR) of Zn(II) complexes suggests that ligand modifications and coordination geometry significantly influence biological activity[6]. However, despite these advancements, limited research has been conducted on the comprehensive spectroscopic, computational[7]. Biological analysis of butane-2,3-dione dioxime and its Zn(II) complex, necessitating further exploration. In this study, butane-2,3-dione dioxime and its Zn(II) complex are synthesized and characterized using various spectroscopic and structural techniques[8]. Including Fourier-transform infrared spectroscopy (FT-IR), ultraviolet-visible (UV-Vis) spectroscopy, proton and carbon nuclear magnetic resonance (^{1}H and ^{13}C NMR) spectroscopy[9]. Powder X-ray diffraction (PXRD), scanning electron microscopy (SEM), and mass spectrometry, to confirm ligand coordination and structural modifications upon complexation[10]. The electronic properties and stability of these compounds are further examined using DFT calculations, which provide insights into their frontier molecular orbital (HOMO-LUMO) energy gaps[11]. Molecular electrostatic potential (MEP) distributions,

and charge delocalization effects upon metal coordination, Molecular docking studies evaluate the binding interactions of the ligand and its Zn(II) complex[12]. With biologically significant proteins, including anticancer (PDB: 1T46) and antioxidant (PDB: 1HD2) targets, to assess their potential therapeutic applications. Additionally, the antimicrobial activity of the synthesized compounds is investigated against bacterial and fungal strains, comparing the efficacy of the free ligand with its Zn(II) complex[13]. By integrating experimental and computational methodologies, this study aims to provide new insights into the coordination chemistry[14]. Electronic behavior, and biological potential of Zn(II)-oxime complexes, contributing to the development of novel metal-based pharmaceuticals and enhancing their applicability in medicinal and bioinorganic chemistry[15].

Experimental Section

Materials and Instruments

Butane-2,3dione-dioxime(98%), hydroxylamine hyhdrochloride (98%), hydrochloric acid (98%), and all metal acetate solid *i.e.* and $Zn(CH_3COO)_2.2H_2O$(98%)were procured from Sigma Aldrich. Solvents used for synthesis and spectroscopic analysis have been used after drying with standard procedures. The elemental analysis of the ligand and metal complex was conducted using a Perkin Elmer (2400) elemental analyzer (Table 1). FT-IR spectra were recorded on a BRUKER FTIR spectrophotometer (4000–400 cm^{-1}) using KBr and polyethylene pellets. Magnetic susceptibilities were measured using Pascal's constant applied for diamagnetic corrections. ^1H and ^{13}C NMR spectra in DMSO-d_6 were recorded on a JEOL JNMECZ-400S (400 MHz) spectrometer with tetramethylsilane as an internal standard. Mass spectra were obtained using an Agilent Q-TOF LC/MS 6530. UV-Vis spectra (200–900 nm) were measured in acetonitrile using a Labindia UV3092 spectrophotometer. Molecular docking simulations were performed using AutoDockVina and PyMOL. Thermal stability was analyzed using a SHIMADZU DTG-60 TGA instrument (25–1000°C) under nitrogen at a 10°C/min heating rate with alumina as a standard. X-ray diffraction (XRD) spectra were recorded on a RigakuMiniFlex system at 22°C (2θ: 0–90°) using a Cu anode source (30 mA, 40 kV), and data were analyzed using X'PertHighScore Plus. DFT optimization of oxime ligands and their complexes was performed using Gaussian09 with B3LYP functionals. Non-metal atoms used 6-31G**(d,p)/ 6-311G**(d,p) basis sets, while Zn(II) used LANL2DZ. The optimized structures were further analyzed for FMO, MEP, and SCF energy, with visualizations generated using Gauss View 6.

Synthesis of oxime ligand and its metal complex

Preparation of ligand

Hydroxylamine hydrochloride (1.39 g, 20 mmol) was dissolved in 20 mL of distilled water in a round-bottom flask and stirred for 20 minutes. A stoichiometric amount of sodium carbonate was then added to the solution, and the reaction mixture was gently heated in a water bath at 30–50 °C to facilitate the evolution of carbon dioxide and the removal of water vapor. Upon cooling to RT, an equimolar amount of 3-(hydroxyimino)butan-2-one (2.32 g, 20 mmol) was added dropwise under continuous stirring with a glass rod. The formation of a white precipitate within 5 minutes indicated the completion of the reaction. The resulting ligand was collected by filtration, washed thoroughly with cold distilled water, and dried under vacuum. The final product was obtained as a white solid in 78% yield (1.81 g), as illustrated in Scheme 1.

Preparation of metal complex

The ligand (2.32 g, 20 mmol) was dissolved in 25 mL of methanol and stirred at RT for 10 minutes. A methanolic solution of zinc(II) acetate dihydrate (4.39 g, 20 mmol) was then added dropwise to the ligand solution under continuous stirring. The reaction mixture was refluxed at 60–70 °C for 3 hours, leading to the gradual formation of a precipitate. The mixture was then cooled to RT, and the solid product was filtered, washed with cold methanol, and dried under

Table 1 — Elemental analysis of ligand and its Zn metal complex

Compound	Colour	Found(C) (calculated)%	Found (N) (calculated)%	Found (H) (calculated)%
Ligand	White	41.37 (41.37)	24.13(24.13)	6.94(6.94)
$ZnC_8H_{16}N_4O_4$ Complex	Pale Green	26.77 (26.77)	15.61 (15.61)	3.37 (3.37)

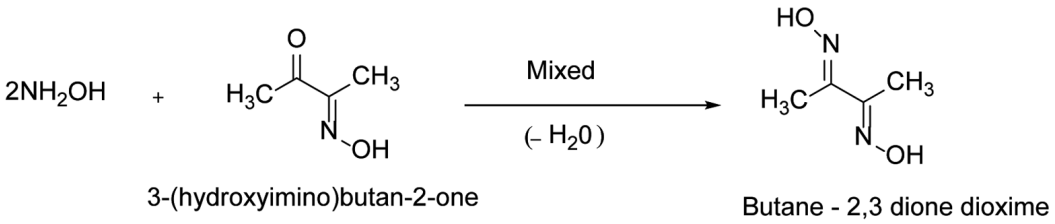

Scheme 1 — Synthesis of oxime ligand

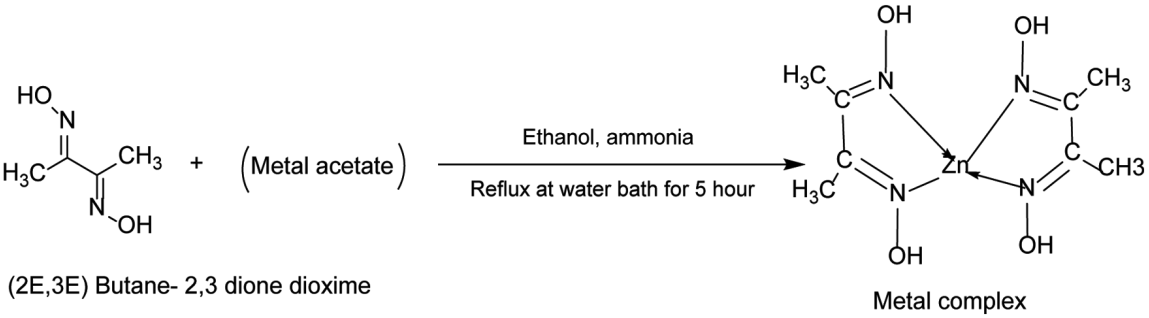

Scheme 2 — Preparation of metal complex

vacuum. The Zn(II) metal complex was obtained in 75% yield (3.62 g), shown in Scheme 2.

Results and Discussion

The produced compounds (Scheme 1 and Scheme 2) exhibit crystalline and non-hygroscopic characteristics. It is insoluble in water but soluble in ethanol, methanol, DMF, and DMSO. The identification and composition of the synthesized compounds were deduced using spectroscopic analyses (IR, UV-Vis, ^{1}H and ^{13}C NMR, TOF-MS), scanning electron microscopy (SEM), antimicrobial assessments, DFT calculations, and molecular docking. The analytical and electronic spectrum data of the ligand and its metal complex suggested a 1:1 metal to ligand stoichiometry.

Spectroscopic Studies

FT-IR Spectroscopy

The FT-IR spectra of butane-2,3-dione dioxime and its Zn(II) complex provide clear evidence of ligand coordination. The O–H stretching band of the free ligand, observed at 3300–3400 cm^{-1}, shifts to 3200–3300 cm^{-1} upon complexation (Fig. 1), suggesting involvement in hydrogen bonding or changes in the electronic environment [16]. The C=N stretching frequency of the oxime group exhibits a downshift from 1620–1650 cm^{-1} to 1580–1600 cm^{-1}, indicating coordination of the oxime nitrogen to the Zn(II) center. A similar shift in the N–O stretching

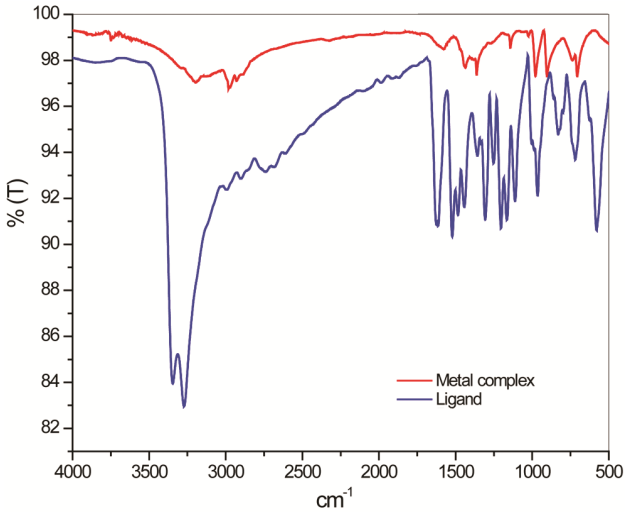

Fig. 1 — FT-IR spectraof Ligand and its Zn metal complex

band from 950–1100 cm^{-1} to 920–1000 cm^{-1} further supports metal-ligand interaction. Additionally, the appearance of a new band at 400–500 cm^{-1} in the complex, absent in the free ligand, confirms the formation of a Zn–N coordination bond [17]. Minor shifts in the aliphatic C–C stretching (1350–1450 cm^{-1}) and methyl bending vibrations (1350–1400 cm^{-1}) were also observed, as summarized in Table 2.

UV-Vis Spectroscopy

The UV-Visible spectrum of the free ligand exhibits absorption bands at 327 nm (n→π*), 286 nm,

and 266 nm (both π→π*), attributed to electronic transitions within the conjugated π-system and the oxime (–C=NOH) functional groups [18]. In the Zn(II) complex, absorption bands are observed at 343 nm, 303 nm, and 275 nm. The red-shifted band at 343 nm corresponds to a ligand-to-metal charge transfer (LMCT) transition, while the bands at 303 nm and 275 nm are attributed to intraligand π→π* transitions, slightly shifted due to complexation-induced electronic changes[19]. The Zn(II) ion, having a d^{10} electronic configuration, is diamagnetic, as it lacks unpaired electrons. Diamagnetic susceptibility measurements, corrected using Pascal's constants, give a total value of -95×10^{-6} cm³ mol⁻¹, confirming the diamagnetic nature of the complex[20]. These findings support the formation of a tetrahedral Zn(II) complex with no d–d transitions, as illustrated (in Fig:S1) and summarized in Table 3.

NMR Spectroscopy

The ^{1}H NMR spectra of butane-2,3-dione dioxime and its Zn(II) complex (in DMSO-d_6) confirm coordination *via* the oxime nitrogen[21]. In the free ligand, the oxime proton appears at 11.48 ppm due to intramolecular hydrogen bonding and electron-withdrawing effects, while methyl protons resonate at 1.97 ppm[22]. Upon coordination with Zn(II), the oxime proton shifts downfield to 10.49 ppm and the methyl signal to 2.26 ppm, indicating changes in the electronic environment upon complex formation (Fig:S2a and S2b).

The ^{13}C NMR spectra further support metal-ligand coordination[23]. The oxime carbon signal in the free ligand appears at 155.42 ppm, which shifts downfield to 134.35 ppm in the Zn(II) complex, confirming coordination through the nitrogen atom[24]. The methyl carbon shifts from 8.32 ppm to 10.62 ppm, while the DMSO solvent peak remains unchanged (~40 ppm)[25]. These chemical shift variations confirm successful coordination of the ligand to Zn(II) *via* oxime nitrogen atoms (Fig:S2c and S2d).

PXRD analysis

Powder X-ray diffraction (PXRD) analysis was employed to assess the crystallinity and structural changes upon complexation of butane-2,3-dione dioxime with Zn(II). The free ligand crystallizes in the orthorhombic system (space group Pnmm) with unit cell parameters a = 14.4180 Å, b = 17.4930 Å, c = 3.9220 Å, and unit cell volume 989.18 Å³. Upon coordination with Zn(II), the complex adopts a monoclinic crystal system (space group $P2_1/n$) with

Table 2 — FT- I R data of ligand and its Zn metal complex

Vibration Mode	Ligand (cm-1)	Zn(II) Complex (cm^{-1})	Assignment
ν (OH) (Hydrogen bonded)	3300-3400	3200-3300	Broad due to H-bonding in free ligand and complex
ν (C=N)(Oxime group)	1629-1650	1580-1600	Shift due to coordination of Zn with oxime group
ν (N-O) (Oxime group)	950-1100	920-1000	Slightly reduced in complex after metal binding
ν (Zn-N)	-	400-500	Metal-to-nitrogen bond in the Zn(II) complex
ν (C-C) (Aliphatic)	1350-1450	1330-1430	Slight shift due to complexation
(C-H) (Methyl group)	1350-1400	1340-1380	In-plane bending, slight shift upon coordination

Table 3 — UV-Vis data of ligand and its Zn metal complex

Compd	Wavelength	Absorbance	Transition	Assignment	Magnetic moment	Geometry
Ligand	327	0.04	n→π*	Lone pair Excitation of Nitrogen /Oxygen in oxime group	-	-
	286	0.58	π→π*	Conjugated π-system transition within the ligand Conjugated π-system transition within the ligand (higher energy		
	266	0.53	π→π*			
Zn Metal complex	343	0.55	π→π*	Ligand – to – Metal charge Transfer	0	Tetrahedral geometry
	303	0.52	π→π* IL transition)	Intraligand Conjugated π-system transition		
	75	0.50	π→π* IL transition)	Intraligand Conjugated π-system transition(higher energy)		

altered unit cell parameters a = 20.5960 Å, b = 6.2230 Å, c = 5.4970 Å, and a reduced unit cell volume of 704.05 Å³, confirming structural reorganization due to metal-ligand coordination[26]. The diffraction pattern (2θ range: 0–90°, Fig. 2) shows enhanced molecular packing in the complex, as reflected by an increase in density from 1.35 g/cm³ (ligand) to 1.69 g/cm³ (complex). Crystallite sizes, estimated using the Debye-Scherrer equation, were 27.65 nm for the ligand and 40.94 nm for the Zn(II) complex, indicating improved crystallinity upon coordination. The calculated and experimental patterns showed excellent agreement using X'Pert HighScore Plus software[27]. PXRD results, including limiting indices, confirm the successful formation of the Zn(II) complex with distinct crystallographic properties (Table 4).

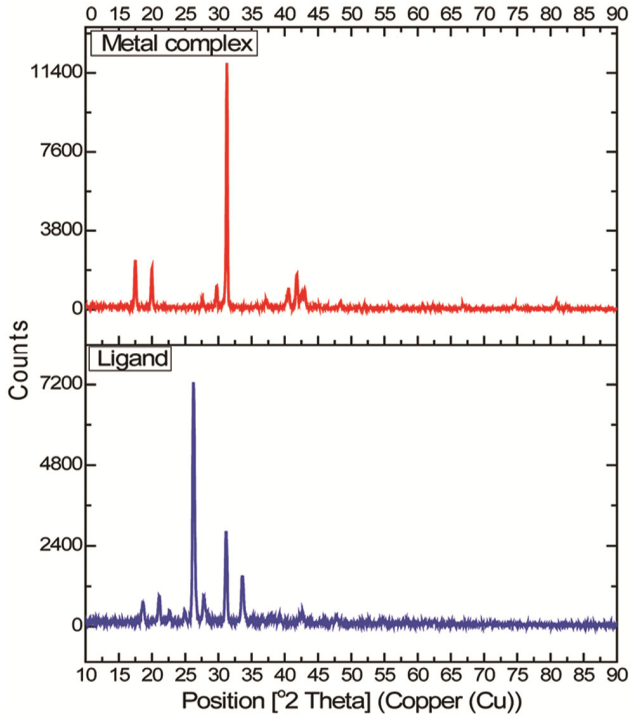

Fig. 2 — PXRD Spectra of ligand and its Zn metal complex

SEM

Scanning Electron Microscopy (SEM) images provide insights into the surface morphology of butane-2,3-dione dioxime and its Zn(II) complex[28]. The ligand displays irregularly shaped crystalline particles with a rough surface at low magnifications (120x and 250x), indicating non-uniform aggregation. At higher magnifications (500x and 1000x), well-defined crystalline facets and layered textures are observed, reflecting its ordered microstructure. In contrast, the Zn(II) complex shows significant morphological changes (Fig. 3a and Fig. 3b). At lower magnifications (230x and 500x), the complex exhibits aggregated, irregular crystalline structures with increased surface roughness, suggesting altered molecular packing due to coordination[29]. At higher magnifications (750x and 1500x), the surface becomes more compact and densely populated with fine granular and needle-like features, indicative of coordination-induced structural rearrangement. These morphological transformations confirm successful complexation and enhanced structural organization in the Zn(II) complex[30].

Table 4 — Powder-XRD of ligand and its Zn metal complex

Empirical formula	Ligand (C4H8N2O2)	Zn Complex (ZnC8H16N4O4)
Formula weight	116	297
Temperature (K)	298	298
wave length (Å)	1.54	1.54
Crystal system	Orthorhombic	Monoclinic
space group	Pnmm	P21/n
unit cell dimensions	a=14.4180 Å b= 17.4930 Å c=3.9220 Å α=β=γ=90°	a= 20.5960 Å b= 6.2230 Å c= 5.4970 Å α=γ=90°, β≠90°
volume (A3)	989.18	704.05
2θ range	0-90°	0-90°
Limiting indices	0<h<1,0<k<1,0<l<1	0<h<2,0<k<2,1<l<1
Density (g/cm3)	1.35	1.69
Z	2.00	2.00
Particle size (nm)	27.65	40.94

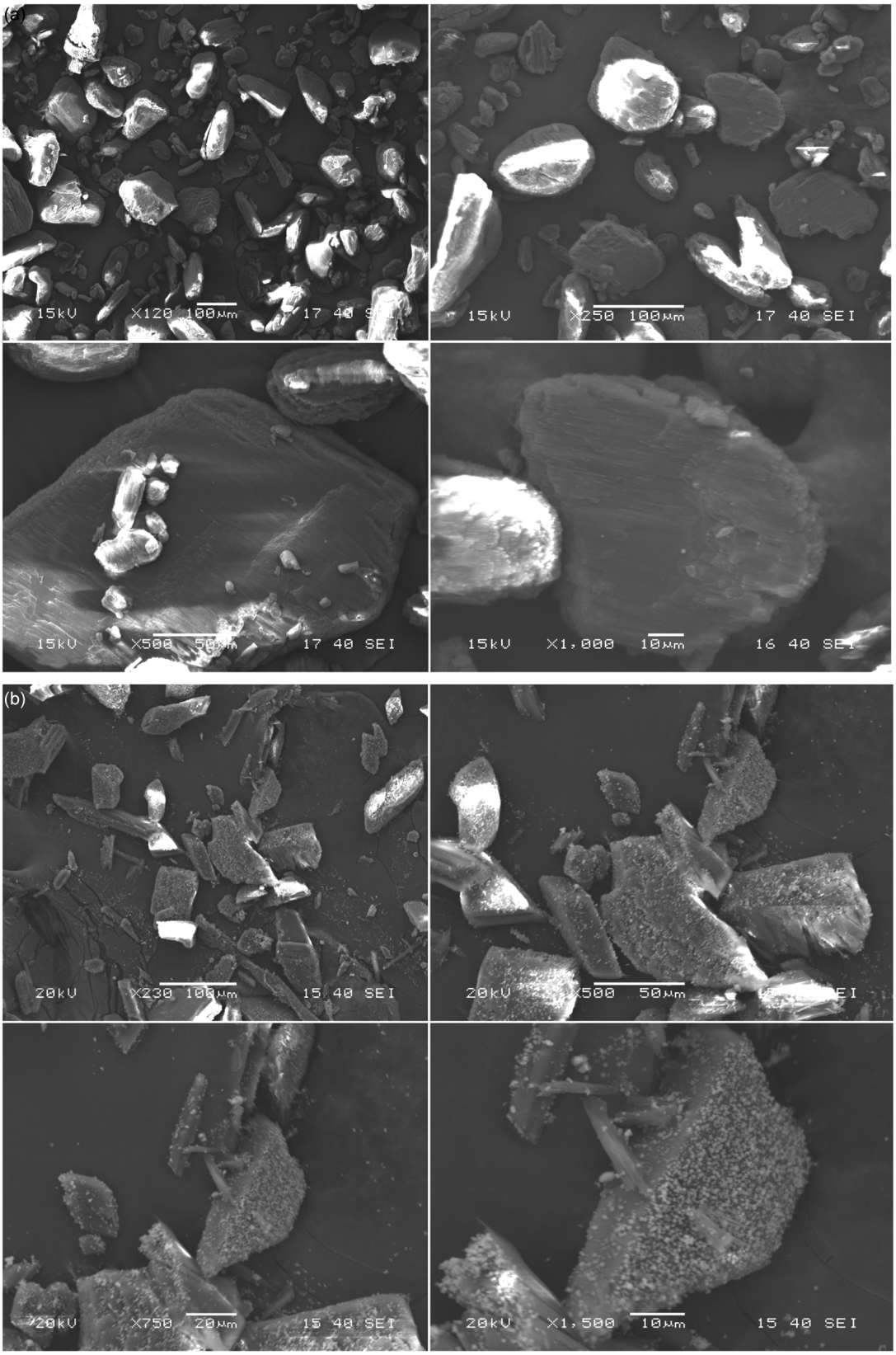

Fig. 3(a-b) — SEM image of ligand; SEM image of Zn metal complex

Table 5 — Bond angle and bond length of ligand and its Zn metal complex

Ligand and Metalcomplexes	Bond	Bond length (Å)	Angle	Bond Angle
Ligand	C_1-N_9	1.319	N_{10}-C_2-C_1	113.821
	N_{10}-C_2	1.320	Zn_{29}-N_9-O_{13}	126.278
	N_{10}-Zn_{29}	2.039	Zn_{29}-N_{12}-C_6	116.546
	O_{14}-N_{10}	1.420	O_{14}-N_{10}-C_2	117.217
	Zn_{29}-N_9	2.031	N_{10}-C_2-C_4	123.28
	N_9-O_{13}	1.420	N_9-C_1-C_3	122.01
	N_{12}-C_6	1.387	C_5-N_{11}-O_{15}	115.838
	C_5-N_{11}	1.386	C_5-C_6-C_8	126.139
	N_{11}-O_{15}	1.487	C_2-C_1-C_3	123.782
	C_2-C_4	1.500	O_{14}-N_{10}-C_2	117.21
	C_1-C_3	1.498	C_6-C_5-C_7	126.141
Zn metal complex	C_1-N_5	1.301	C_1-N_5-O_7	110.682
	N_5-O_7	0.978	C_2-C_1-C_3	121.102
	C_1-C_3	1.479	C_4-C_3-N_6	124.823
	C_1-C_2	1.502	C_3-N_6-O_8	117.097
	C_3-C_4	1.516		
	C_3-N_6	1.304		
	N_6-O_8	1.422		

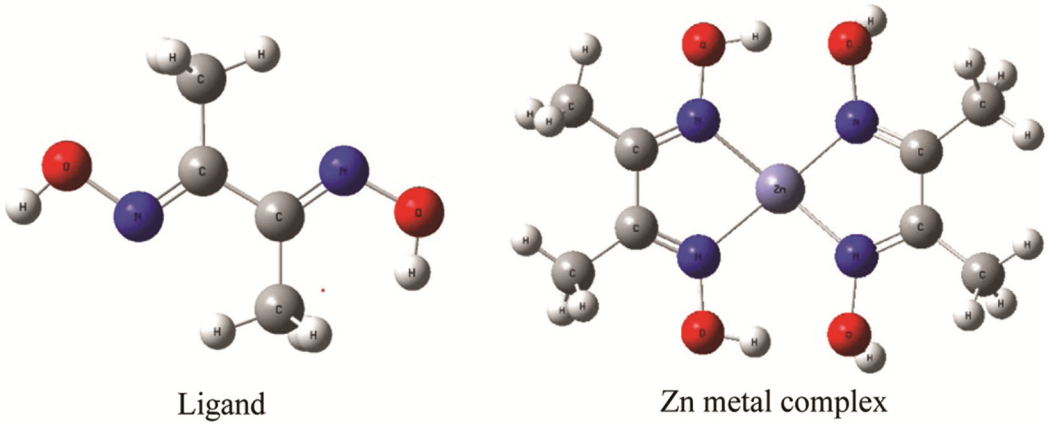

Fig. 4 — Optimized Structure of ligand and its Zn metal complex

Molecular Modeling/ DFT Calculations

Density Functional Theory (DFT) calculations were performed to investigate the structural and electronic properties of butane-2,3-dione dioxime and its Zn(II) complex. Geometry optimizations were carried out using the RBLYP functional with 6-31G**(d,p) and 6-311G**(d,p) basis sets for the ligand and the LANL2DZ pseudopotential for Zn(II), accounting for relativistic and core-electron effects. The optimized geometry of the free ligand yielded a total energy of −550.47 Hartree and a dipole moment of 5.20 Debye, indicating significant electronic polarization[31]. The ligand belongs to the C_1 point group, reflecting its asymmetrical structure. Calculated bond lengths and angles (Table 5) define its structural configuration (Fig. 4). For the Zn(II) complex, the optimized energy was −2613.07 Hartree with a reduced dipole moment of 1.51 Debye, signifying decreased polarity upon coordination. The complex also falls under the C_1 point group, confirming low symmetry. Structural distortions in bond lengths and angles upon coordination highlight the ligand–metal interaction and confirm successful complexation[32].

Frontier Molecular Orbitals and Molecular Electrostatic Potential

Frontier Molecular Orbitals (FMO) study revealed the ligand and Zn(II) metal complex's electronic characteristics and reactivity[33]. Calculations were made for the LUMO and HOMO energies. The ligand's LUMO energy was –0.05495 eV and its

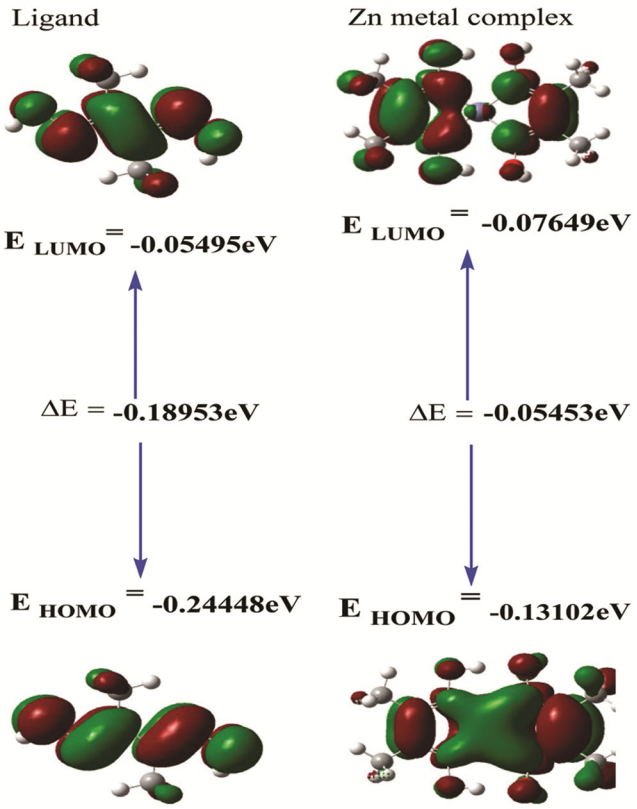

Fig. 5 — Energies of HOMO and LUMO of ligand and its Zn metal complexes

HOMO energy was –0.24448 eV, creating an energy gap of –0.18953 eV. LUMO energy was –0.07649 eV and HOMO energy was –0.13102 eV in the Zn(II) metal complex, (shown in Fig. 5) reducing the energy gap by –0.05453 eV. Electronic delocalization and potential reactivity rise with this considerable energy gap decrease during complexation. MEP analysis showed the ligand and metal complex charge distribution. The MEP map of the ligand showed a strongly negative electrostatic potential region (red area) with a value of –6.223 e^{-2} and a highly positive region (blue area) with 6.223 e^{-2}. After complexation with Zn(II), the electrostatic potential values shifted to –5.415 e^{-2} in red and 5.415 e^{-2} in blue (shown in Fig. 6). Coordination with the metal center redistributes electron density, which can affect intermolecular interactions and reactivity[34].

Total SCF Density

The overall Self-Consistent Field (SCF) density reveals a molecule or complex's electronic dispersion and charge delocalization[35]. SCF density pictures of the free ligand and its Zn(II) metal complex show considerable electron density changes during complexation[36]. The free ligand's SCF density contours show a highly delocalized electron cloud with high electron density around the oxygen (red spheres) and nitrogen (blue spheres) atoms. The electron-rich oxime (-C=NOH) functional groups are essential for metal coordination. After complexation with Zn(II), SCF density changes significantly. The Zn(II) complex has a more symmetrical electron density and improved charge delocalization throughout the molecular framework. SCF density contours show that Zn(II) cooperation with the ligand redistributes electron density around the metal center. The metal ion and ligand interaction increases electron density at Zn coordination sites, stabilizing the complex(shown in fig: S3). The strong Lewis acidic character of Zn(II) removes electron density from donor atoms (oxygen and nitrogen), causing this redistribution. This improves metal-ligand bonding and complex structure[37].

Molecluar Docking of ligand and its Zn(II) metal complex

Molecular Docking with Anticancer Protein (PDB: 1T46)

Molecular docking studies were carried out using AutoDock Vina to assess the binding interactions of

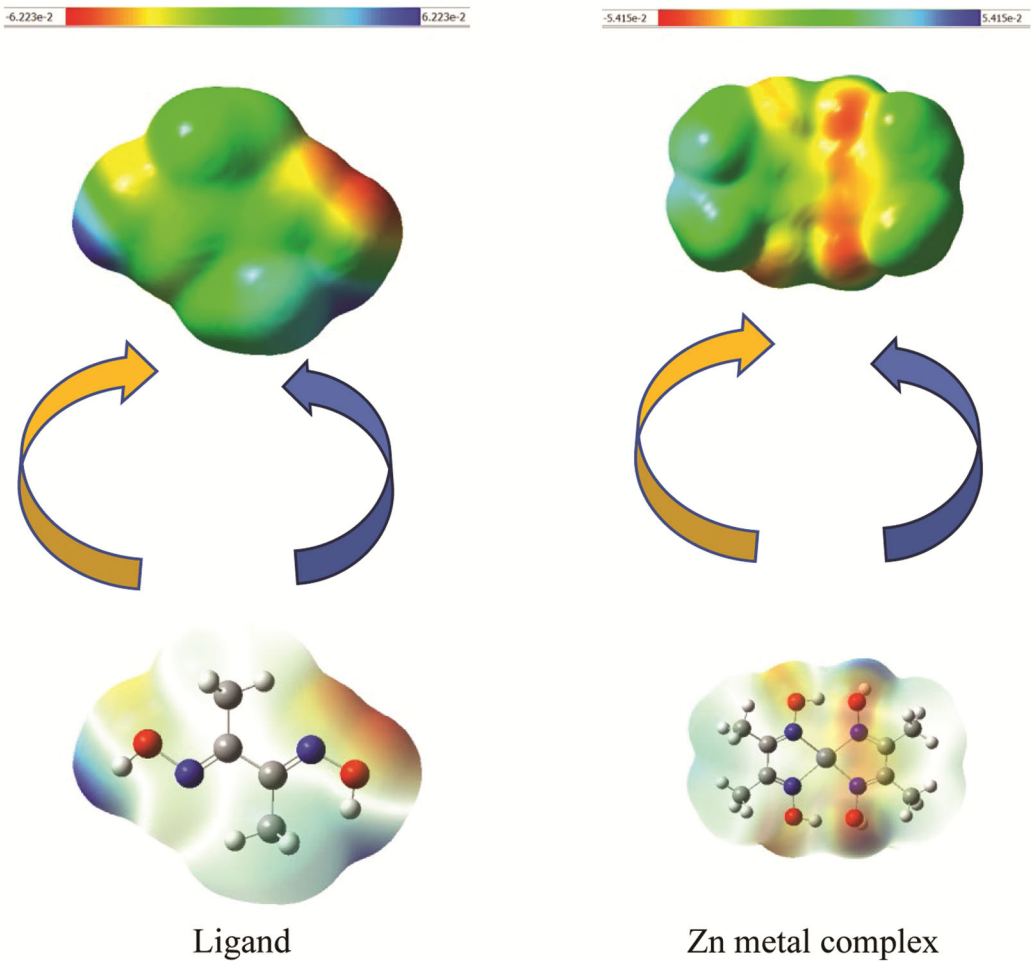

Fig. 6 — MEP analysis of ligand and its Zn metal complex

butane-2,3-dione dioxime and its Zn(II) complex with the anticancer target protein (PDB ID: 1T46). Structural visualizations and interaction analyses were performed using PyMOL[38]. The free ligand exhibited a higher binding affinity with a docking score of −9.48 kcal/mol and an inhibitory constant (Ki) of 133.38 µM, indicating strong interaction with the active site. In contrast, the Zn(II) complex showed a reduced binding energy of −4.99 kcal/mol and a Ki of 221.64 µM, suggesting decreased affinity due to conformational changes upon metal coordination (Table 6). Hydrogen bonding and electrostatic interactions contributed significantly to complex stability[39]. The free ligand formed multiple stable hydrogen bonds with key amino acid residues, enhancing its binding efficiency. Docking poses and conformational changes were visualized in ribbon and bubble models (Fig:S4, Fig. 7a), highlighting differences between the ligand and its Zn(II) complex[40].

Molecular Docking with Antioxidant Protein (PDB: 1HD2)

Molecular docking simulations were performed to investigate the binding interactions of butane-2,3-dione dioxime and its Zn(II) complex with the antioxidant protein (PDB ID: 1HD2). The free ligand displayed a stronger binding affinity, with a binding energy of −7.33 kcal/mol and an inhibitory constant (Ki) of 202.72 µM, compared to the Zn(II) complex, which showed a binding energy of −5.26 kcal/mol and Ki of 238.84 µM (Table 6). Electrostatic energy of 0.48 kcal/mol in the Zn(II) complex indicated partial stabilization *via* charge interactions. The observed decrease in binding affinity upon complexation suggests structural and electronic modifications influencing ligand-protein recognition. Partition constant (Q) variations implied altered solubility and hydrophobic properties due to metal coordination. Hydrogen bonding analyses identified key active-site residues contributing to complex stability.

Table 6 — Molecular docking with anticancer and antioxidant protein of ligand and its Zn metal complex interaction

S. No.	Chemical Properties	Ligand + Anticancer proteins (PDB=1T46)	Zn (II)Complex + Anticancer proteins (PDB=1T46)	Ligand+ Antioxidant proteins (PDB=1HD2)	Zn (II) Complex + Antioxidant proteins (PDB=1HD2)
1	Grid energy	1000.00	1000.00	1000.00	-1000.00
2	Binding Energy(Kcal/mol)	-9.48 Kcal/mol	-4.99Kcal/mol	-7.33Kcal/mol	-5.26 Kcal/mol
3	Electrostatic energy	0.00Kcal/ mol	0.34Kcal/ mol	0.00 Kcal/mol	0.48 Kcal/mol
4	Inhibitory constant	133.38 µm	221.64 µm	202.72µm	238.84 µm
5	Partition constant(Q)	152.27Kcal/mol	50.38 Kcal/mol	50.41 Kcal/mol	50.40 Kcal/mol
6	Free energy (A)	-2977.59K cal/mol	-2322.27 Kcal/mol	-2975.37 Kcal/mol	2322.54 Kcal/mol
7	Internal energy(U)	-8.88 Kcal/mol	-4.47 Kcal/mol	-6.66 Kcal/mol	-4.74 Kcal/mol
8	Entropy (S)	9.96 Kcal/mol	7.77 Kcal/mol	9.96 Kcal/mol	7.77 Kcal/mol
9	Torsional free energy	1.19 Kcal/mol	0.89 Kcal/mol	1.19 Kcal/mol	1.19 Kcal/mol
10	Intermolecular energy	-10.57 Kcal/mol	-5.88 Kcal/mol	-8.52 Kcal/mol	-6.13 Kcal/mol
11	Unbound system energy	-2.53 Kcal/mol	0.15 Kcal/mol	-1.95 Kcal/mol	0.15 Kcal/mol
12	Grid dimension	28.331, 26.863 37.278	7.970, 42.638, 20.192	7.970, 42.632, 20.192,	47.941, 46.030, 13.154,
13	Grid spacing	0.375 Å	0.375 Å	0.375Å	0.375 Å

Conformational differences were visualized through ribbon and bubble models (Fig:S5 and Fig. 7b), highlighting the ligand's structural adaptability upon interaction with the antioxidant target[41].

Biological Activity of ligand and its Zn(II) metal complex

Antifungal Activity

The antifungal activity of butane-2,3-dione-dioxime and its Zn(II) metal complex was evaluated against *Aspergillus niger* (*A. niger*), using Amphotericin B as the standard antifungal agent. The Minimum Inhibitory Concentration (MIC) values indicate that the ligand exhibited significant antifungal activity, with an MIC value of 0.05 µg/mL. The Zn(II) metal complex displayed a slightly reduced antifungal potency compared to the free ligand, with an MIC of 0.06 µg/mL[42]. However, both the ligand and its metal complex showed superior antifungal efficacy compared to the standard *Amphotericin B,* which exhibited an MIC value of 0.5 µg/mL. The reactivity order based on MIC values for antifungal activity follows:Ligand (0.05 µg/mL) > Complex (0.06 µg/mL) >*AmphotericinB* (0.5 µg/mL, Fig. 8a). The dose-dependent inhibition pattern observed in the antifungal assay further supports the potential application of these compounds as antifungal agents, with the ligand demonstrating a slightly higher efficacy than the Zn(II) complex (Table 7). The enhanced activity of the ligand over its metal complex suggests that complexation may influence the interaction with fungal targets, potentially due to changes in solubility, bioavailability, or mechanism of action[43].

Antibacterial Activity

The antibacterial efficacy of butane-2,3-dione-dioxime and its Zn(II) metal complex was assessed against *Escherichia coli* (*E. coli*), with *Ciprofloxacin* serving as the standard reference drug[44]. The ligand demonstrated excellent antibacterial activity with an MIC of 0.08 µg/mL, significantly lower than *Ciprofloxacin* (MIC = 5 µg/mL), indicating its strong potential as an antibacterial agent. The Zn(II) complex exhibited a slightly reduced antibacterial activity with an MIC value of 0.9 µg/mL, which is still more potent than the standard drug *Ciprofloxacin*. The reactivity order based on MIC values for antibacterial activity follows:Ligand (0.08 µg/mL) > Complex (0.9 µg/mL) >*Ciprofloxacin* (5 µg/mL, Fig. 8b). The metal complex demonstrated enhanced activity at higher concentrations, suggesting that complexation plays a crucial role in modulating the antibacterial effect[45]. The greater efficacy of the free ligand compared to the complex may be attributed to better interaction with bacterial cellular components[46]. whereas the Zn(II) complex might require specific conditions for optimal activityThe results suggest that

(a)

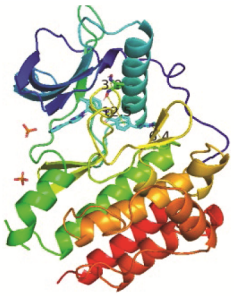

Ligand interaction with protein (1T46)

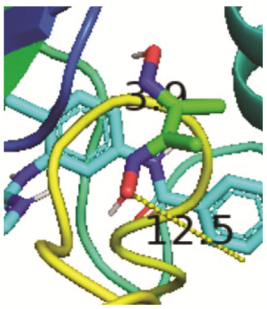

Zoom structure of ligand and protein interaction

Zn metal complex interaction with protein (1T46)

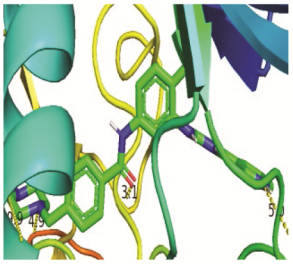

Zoom structure of Zn metal complex and protein interaction

(b)

Ligand interaction with protein (1HD2)

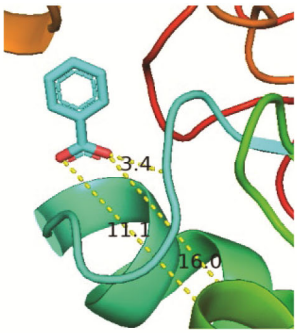

Zoom structure of ligand and protein interaction

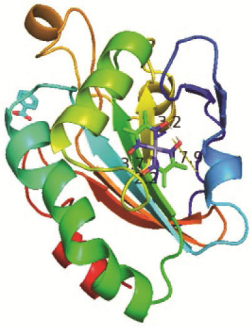

Zn metal complex interaction with protein (1HD2)

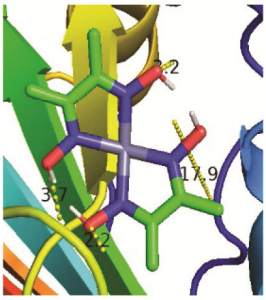

Zoom structure of Zn metal complex and protein interaction

Fig. 7 (a -b) — Ligand and Protein binding interaction (Ribbon structures) anticancer protein (PDB-1T46); Ligand and Protein binding interaction (Ribbon structures) with Antioxidant protein (PDB-1HD2)

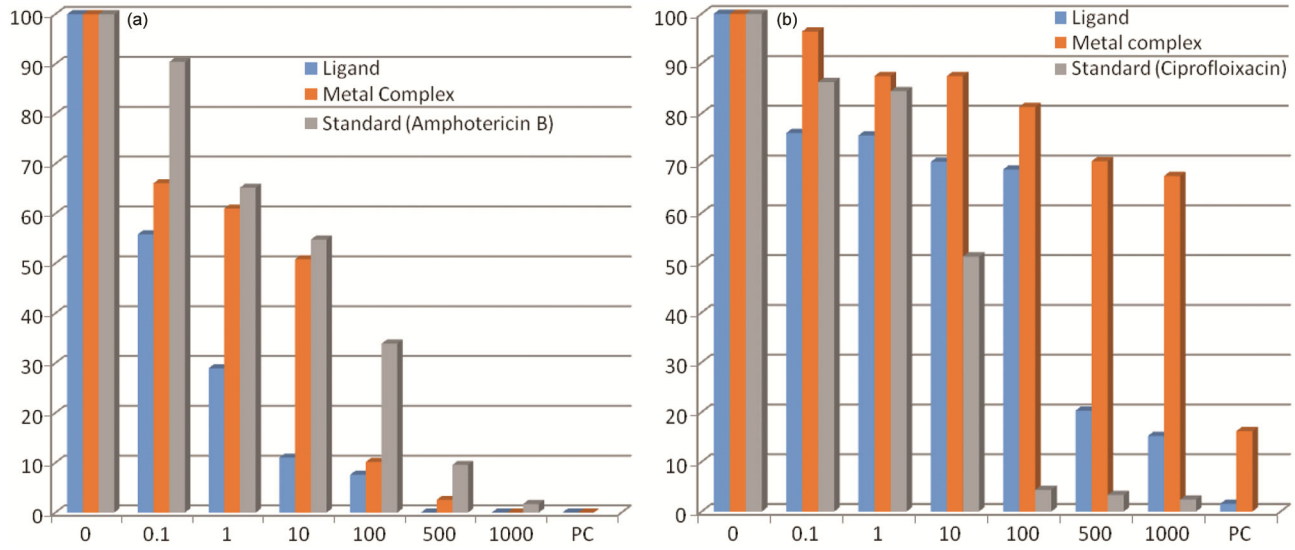

Fig. 8(a- b) — Antifungal activities of ligand and its Zn metal complex; Antibacterial activities of ligand and its Zn metal complex

Table 7 — Antimicrobial activities of ligand and its Zn metal complex

S. No.	Compd	Bacterial strain *E.coli* MIC (µg/mL)	Fungal strain *A.niger* MIC (µg/mL)
1	Ligand	0.08 µg/mL	0.05 µg/mL
2	Complex(I)	0.9 µg/mL	0.06µg/mL
4	*Ciprofloxacin*	5µg/mL	-
5	*Amphotericin B*	-	0.5µg/mL

butane-2,3-dione-dioxime and its Zn(II) complex could serve as promising antibacterial agents with potent activity against *E. coli,*(Table 7).

Conclusion

This study successfully synthesized and characterized butane-2,3-dione dioxime and its Zn(II) complex, providing a detailed investigation of their structural, spectroscopic, computational, and biological properties. FT-IR, UV-Vis, NMR, PXRD, SEM, and mass spectrometry confirmed the coordination of the oxime ligand to Zn(II) *via* nitrogen atoms, leading to notable shifts in vibrational and electronic transitions. PXRD analysis revealed improved crystallinity and increased molecular packing upon complexation. DFT calculations demonstrated a reduced HOMO-LUMO gap in the Zn(II) complex, suggesting enhanced stability and electronic delocalization, while molecular electrostatic potential (MEP) analysis indicated significant charge redistribution due to metal coordination. Molecular docking studies showed that butane-2,3-dione-dioxime had stronger binding affinities toward anticancer (PDB: 1T46) and antioxidant (PDB: 1HD2) proteins compared to its Zn(II) complex, highlighting the ligand's potential in drug design. Antimicrobial activity assessments revealed that the free ligand exhibited higher antibacterial and antifungal efficacy than the Zn(II) complex, likely due to better interaction with microbial targets. These findings suggest that while the ligand demonstrates strong bioactivity, complexation with Zn(II) alters its biological properties, possibly influencing its mechanism of action. This study advances the understanding of Zn(II)-oxime coordination chemistry and its bioactive potential, paving the way for future research into structural modifications and hybrid metal complexes to enhance therapeutic applications in medicinal and bioinorganic chemistry.

Declaration of Competing Interest

The author declare that they have no known competing financial interests or personal relationships that could have appeared to influence the work reported in this paper.

Supplementary Information

Supplementary information is available in the website http://nopr.niscpr.res.in/handle/123456789/58776.

Acknowledgments

For providing analytical facilities, Authors are thankful to Nano Science Department of Chemistry DSB Campus Nainital, University of Delhi, India for their cooperation in recording the spectra of the synthesized compounds and Aakaar Biotechnologies Private Limited company Lucknow (India) for antimicrobial study.

References

1 Korkmaz Ü, Findik B.T, Dede B & Karipcin F, *Bioorg Chem*, 121 (2022) 105685.
2 Chahar M M, Choudhary N, Yadav K K, Qasim M.T, Zairov R, Patel A, Yadav V.K & Jangir M, *J Iran Chem Soc*, 22 (2025) 1.
3 Mucha P, Skoczyńska A, Małecka M, Hikisz P & Budzisz E, *Molecules*, 26 (2021) 4886.
4 Jain G, Chaurasia R, Kaur B P, Chowdhury O P, Roy H, Gupta R.R, Biswas B, Chakrabarti S & Mukherjee M, *J Mat Chem B*, 13 (2025) 3270.
5 Fouad R, Mahdi M A N & Adly O M I, *App Organomet Chem*, 39 (2025) e7840.
6 Damena T, Alem M B, Zeleke D, Desalegn T, Eswaramoorthy R & Demissie T B, *Front Chem*, 10 (2022) 1053532.
7 Kassem A, Abbas L, Coutinho O, Opara S, Najaf H, Kasperek D, Pokhrel K, Li X & Tiquia-Arashiro S, *Microbiol*, 14 (2023) 1304081.
8 Shahbahram S A & Abdulkareem I I, *J Pure App Sci*, 35 (2023) 177.
9 Murugan S, Ashokan A, Velmurugan Y, Rajakannan V, Khamrang T, Savaridasson J K, Subramanian U M & Hemamalini M, *J Mol Struc*, 1321 (2025) 140010.
10 Alshater H, El-Boraey H A, Homoda A M & EL-Gammal O A, *J Mol Struc*, 1232 (2021) 129985.
11 Wang Z, Fang Z, Liu L & Wu T, *J Mol Model*, 29 (2023) 326.
12 Khalaf M M, El-Lateef H M A, Gouda M, Abdelhamid A A, Abdelbaset M, Alsulami A H, Almarri M N & Abdou A, *Comp Biol Chem*, 109 (2024) 108031.
13 El-Lateef H M A, Ali A M, Khalaf M M & Abdou A, *Bull Chem Soc Ethiop*, 38 (2024) 147.
14 Farooq U, Bukhari S M, Khan S, Xu X-L, Xu H-G & Zheng W-J, *Coord Chem Rev*, 517 (2024) 216041.
15 Omer P.K, Aziz N.M & R.A. Omer, *Rev Inorg Chem*, 44 (2024) 699.
16 Rathika A, Reeda V J & Divya P, *J Mol Struc*, 1310 (2024) 138231.
17 Schubert U S, Behrendt F & Gottschaldt M, *Mat Horiz*, 11 (2024) 4600.
18 Rizk M G, Emara A A, Abou-Hussein A A & Mahmoud N H, *J Mol Struct*, 1277 (2023) 134816.
19 Irshad R, Asim S, Mansha A & Arooj Y, *J Fluoresc*, 33 (2023) 1273.
20 Urien E R, Switchable iron (II) coordination polymers for multifunctional applications, (2022). (https://hdl.handle.net/20.500.14352/3717).
21 Cain C F, Synthesis of Biologically Relevant Compounds Harboring Unusual Hydroxamate or Proline Amino Acid Residues, University of Notre Dame, 2023. https://search.proquest.com/openview/455af0474899970450d06c9b1c065388/1?pq-origsite=gscholar&cbl=18750 & diss=y.
22 Adam A M A, Hegab M S, Refat M S & Eldaroti H H, *J Mol Struc*, 1231 (2021) 129687.
23 Salem N M, Foro S & Iskander M F, *J Mol Struc*, 1227 (2021) 129571.
24 Chahal S, Punia J, Rani P, Singh R, Kumar P, Kataria R, Joshi G & Sindhu J, *RSC Med Chem*, 14 (2023) 757.
25 Serbest K, Dural T, Emirik M, Zengin A & Faiz Ö, *J Mol Struc*, 1229 (2021) 129579.
26 Keri R S, Reddy D, Budagumpi S & Adimule V, *RSC Adv*, 13 (2023) 20373.
27 Nikseresht A, Ghoochi F & Mohammadi M, *ACS Omega*, 9 (2024) 28114.
28 Murphy O, Optimizing the fabrication process for next generation nano-textured solar cells with high conversion efficiency using industrially viable solar cell processes, (2022). https://arrow.tudublin.ie/scienmas/106/.
29 Osman A I, Ayati A, Krivoshapkin P, Tanhaei B, Farghali M, Yap P.-S & Abdelhaleem A, *Coord Chem Rev*, 514 (2024) 215900.
30 Khan S, Akhtaruzzaman, Medishetty R, Ekka A & Mir M H, Chem Asian J, 16 (2021) 2806.
31 Luo H & Liu J, *Ange Chem Int Ed*, (2024) e202410759. https://doi.org/10.1002/anie.202410759.
32 Tahara K, Morino T, Morimoto Y, Nakamura Y, Sugimoto K, Ozawa Y & Abe M, *Inorg Chem*, 63 (2024) 19087.
33 Akbari Z, Stagno C, Iraci N, Efferth T, Omer E.A, Piperno A, Montazerozohori M, Feizi-Dehnayebi M & Micale N, J Mol Struct. 1301 (2024) 137400.
34 Sarkar M, *Inorganica Chim Acta*, 572 (2024) 122275.
35 Hardikar T S, Self Consistent Excited State Mean Field Theory: Development and Applications, University of California, Berkeley, 2023. https://search.proquest.com/openview/a655c49bde388f92fd197074211cbde5/1?pqorigsite=gscholar&cbl=18750&diss=y.
36 Boshra M, Adly O M I, Abdelrhman E M, Eid M F & Samy F, *Appl Organomet Chem*, 38 (2024) e7752.
37 Obeso J L, Huxley M T, Leyva C, Flores J G, Martín-Guaregua N, Viniegra M, Aguilar-Pliego J, Reyes J A de los, Ibarra I A & Peralta R.A, *Coord Chem Rev*, 496 (2023) 215403.
38 Mao T, Chen B, Wei W, Chen G, Liu Z, Wu L, Li X, Pathak J L, Li J, *Heliyon*, 10 (2024) 09891.
39 Salha D, Andaç M, Denizli A, *J Mol Recog*, 34 (2021) e2875.
40 Firdaus S, M. Amir, Ahmad A, Ali A, Alam M J, Dilshad S, Javed S & Ahmad M, *J Biomol Struc Dyn*, 42 (2024) 8307.
41 Sahu G, Banerjee A, Samanta R, Mohanty M, Lima S, Tiekink E R T & Dinda R, *Inorg Chem*, 60 (2021) 15291.
42 Aljohani E T, Shehata M R, Alkhatib F, Alzahrani S.O & Abu-Dief A.M, *App Organomet Chem*, 35 (2021) e6154.
43 Pandey A & Boros E, *Chem Eur J*, 27 (2021) 7340.
44 Ahmed M, Chand R & Singh B K, *J Coord Chem*, 77 (2024) 2217.
45 Bagul A, Kumar M, Tufail A, Tufail N, Gaikwad D & Dubey A, *App Organomet Chem*, 38 (2024) e7521.
46 Khalaf M M, El-Lateef H M A, Taha A A & Abdou A, *Appl Organomet Chem*, 39 (2025) e70027.